

Mode conversion noise attenuation, modelling and removal: case studies from Cyprus and Egypt

Jyoti Kumar^{1*}, Marcus Bell¹, Mamdouh Salem¹, Tony Martin¹ and Stuart Fairhead¹ propose a method to attenuate converted mode energy to improve the imaging for prospective sub-salt targets.

Introduction

The wavefront from a source that strikes an acoustic impedance contrast separates into four variables: transmitted and reflected compressional waves (P-wave) and transmitted and reflected shear waves (S-wave). Converted waves are those whose mode changes at the interface and can be recorded in a marine environment in the presence of large velocity contrasts. The difference in acoustic velocities at the boundary means that in high contrast media the distinction between compressional and shear velocities across the boundary is small; shear waves are not as refracted as compressional waves and can be recorded as partially converted reflected energy.

The eastern Mediterranean contains two major sedimentary basins, the Levantine and Herodotus (see Figure 1). They have shared depositional regimes and therefore contain similar sedimentary sequences. The Levantine Basin sits offshore Cyprus, Israel, Palestine and Lebanon, and was formed by prolonged phased rifting, with subsequent subsidence and loading by deltaic sediments (Gradmann et al., 2005; Gardosh and Druckman, 2006). It forms a northeast-oriented depression about 2 km deep and contains more than 14 km of Mesozoic and Cenozoic

sequences that include up to 2 km of Messinian salt (Druckman et al., 1995; Ben-Avraham et al., 2002; Netzeband et al., 2006). The local reservoirs include both Cretaceous and Jurassic sandstones and limestones, with older potential reservoirs in the Triassic sandstones. Shales and marls of Paleogene, Neogene, Cretaceous and Jurassic, along with Messinian salt and Triassic evaporites all form local seals (Roberts and Peace, 2007) in plays of a both stratigraphic and structural nature.

The Herodotus Basin is a northeast trending 3 km deep depression, and represents a slab of the Early Mesozoic Neo-Tethys Ocean (see Figures 1 and 2). The basin is bounded on the north by the Mediterranean Ridge; on the northeast by the west portion of the Cyprus Arc and on the south by the Nile Delta cone. The Eratosthenes Seamount (ESM), a fragment of continental crust (Robertson, 1998), forms the eastern limit of the Herodotus Basin, and additionally delineates the boundary between the cone of the Nile Delta, the Herodotus Basin, and the Levant Basin. The Herodotus Basin itself contains up to 7 km of Mesozoic–Cenozoic sediment (Voogd and Truffert, 1992; Garfunkel, 1998), and is overlain by up to 3 km of Messinian salt (Garfunkel, 1998; Aal et al., 2000; Loncke et al., 2006).



Figure 1 Map showing the structural detail of East Mediterranean area.

¹ PGS

* Corresponding author, E-mail: jyoti.kumar@pgs.com

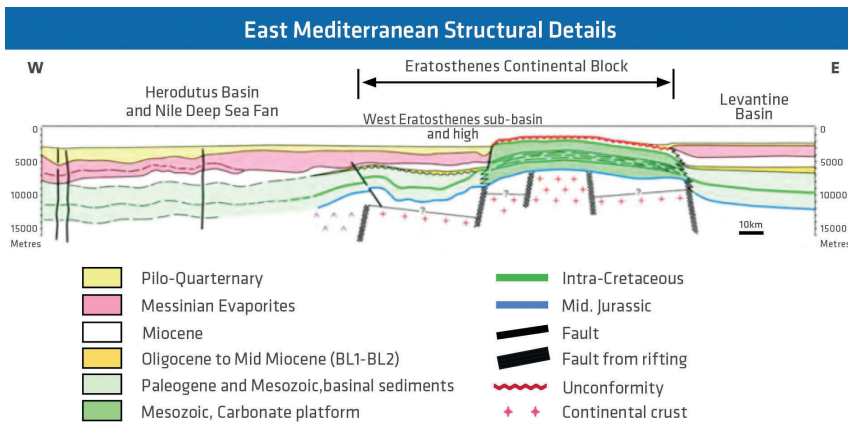


Figure 2 Section showing the structural detail of East Mediterranean area.

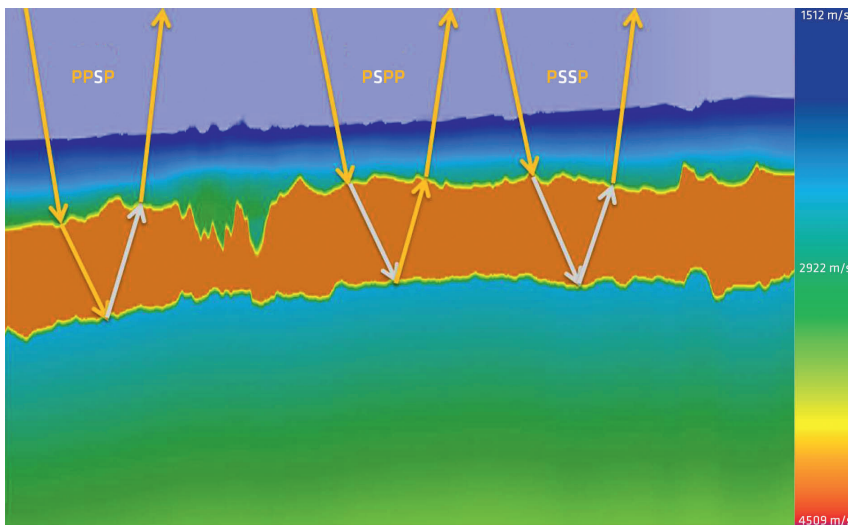


Figure 3 Three possible converted wave ray paths generated from a salt layer (PPSP, PSPP and PSSP).

Figure 2 shows the chronological representation of the basin sediment fill, which are divided into Mesozoic and Paleogene sediments, pre-Messinian sediments (Miocene), Messinian evaporites, and Plio-Pleistocene-Quaternary sediments. The Messinian evaporites originated during the closing of Gibraltar, with thicknesses reaching 3 km. The structure of the evaporites can be dome shaped from syndepositional folding or diapiric, after deformation and movement. The overburden Plio-Pleistocene-Quaternary deposits consist of sediments rich in carbonate material. These laminated deposits are rich in organic material, sapropels, and turbidites. One class of turbiditic sands were transported through the five main Nile submarine channels; these are considered a primary target for hydrocarbon prospectivity.

The presence of a Messinian salt layer in this region creates large velocity contrasts between the salt and surrounding sediments. This can generate uncertainty in imaging around potential prospects (Elbassiony et al., 2018). Single value P-wave velocities for the salt in this region are approximately 4200 m/s, whereas the sediment velocity in the post-Messinian overburden and pre-Messinian range from 2400 to 3000 m/s. This strong acoustic velocity contrast at the top and base of salt layer often results in mode conversion. Many prospects in this region are sub-salt, frequently in the vicinity of the recorded converted mode energy. Suppressing this energy has a strong positive impact on the interpretation of potential prospects, particularly in revealing play delineation, but also enabling more accurate

amplitude analysis (AVA) of pre-stack data. It can also assist in improving velocity model building (VMB). In this paper we proposed a method to suppress this energy by modelling the converted wave energy using 3D acoustic modelling.

Method

Defining the problem

Converted mode contamination of P-wave images is a well-known and pernicious problem in some geological settings. In salt provinces, the large velocity contrast between the salt and surrounding sediments generates conversion between P-wave and S-wave energy. This often results in recording of converted mode events. Because the converted mode has a slower apparent velocity, the converted energy occurs deeper than the high contrast boundary and can obscure data interpretability and potential prospectivity. The mode conversion to S-wave is created at steeply dipping salt interfaces, and converts back to a P-wave on the upcoming wavefront (Ogilvie and Purnell, 1996; Lu et al., 2003). These undesired contaminants of the image can sometimes be exploited to aid in the interpretation of the base of salt, as they offer enhanced illumination owing to different angular coverage (Jones and Davison, 2014). However, as this energy can act as noise on P-wave migrated images, generally there is a need to suppress them to facilitate interpretation.

The converted waves examined in this paper are those which convert to S-waves at the top and base of salt and travel outside

the salt as P-waves. As shown in Figure 3, three possible converted modes of base salt are PSPP, PPSP and PSSP. The arrival time for symmetrical mode PSSP will be significantly larger than those of an asymmetrical mode, like PSPP and PPSP, as S-waves travel slower than P-waves. In addition, the symmetrical mode will be recorded with much weaker amplitude. This is owing to the smaller velocity contrast between S-wave salt velocity and surrounding P-wave sediment velocities. In some cases a symmetrical mode is not observed in the recorded field data because of its amplitude being much lower than the P-wave amplitudes recorded at the same two-way time. In this case suppression of asymmetrical modes such as PSPP and PPSP are sufficient to improve the sub-salt imaging.

Existing methods to suppress converted modes include filtering the offending energy based on normal move-out velocity, as converted waves travel with a slower S-wave component (Ogilvie and Purnell, 1996), or surgical muting of energy using travel time ray-tracing (Lu et al., 2003). The effectiveness of both these methods could be significantly reduced in the presence of complex

salt geometries. Dual-leg 3D acoustic modelling has been proposed to model converted wave energy (Huang et al., 2013), which was subsequently used to attenuate it from a pre-migration or post-migration dataset. In the presence of complex salt geometries, diffractions from the top salt interfere with the converted mode generated by the base salt, modelled during forward propagation. This makes it difficult to subtract the converted wave energy before migration. In this paper we perform 3D acoustic modelling twice, with and without the base salt interface in the velocity model used for the propagation. This generates a much cleaner converted wave model that can be subtracted from both pre-stack and pre-migration gathers more effectively.

Solution

The ratio (r) between the salt thickness in time (Δt_{salt}) and the time interval between P-wave and converted-wave base salt (Δt_{cw}) on time migrated data can be used to identify whether the converted mode has propagated as an S-wave on one or both of the down-going and up-coming wave-fields within the salt.

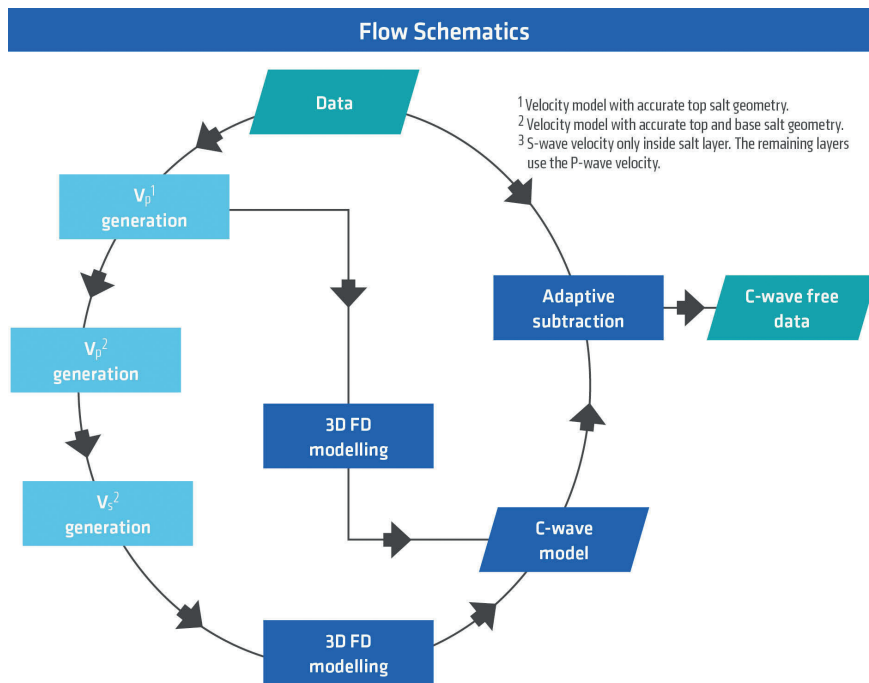


Figure 4 Conceptual overview of the converted wave (C-wave) attenuation methodology.

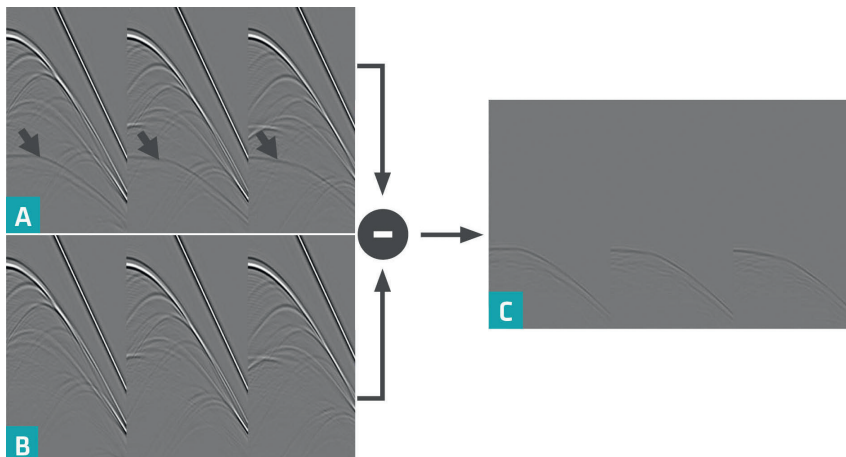


Figure 5 Different stages of modelling: 3D acoustic forward modelling with the base salt reflector included in the modelling (a); forward modelling without the base salt reflector in the model (b) and a subtraction of the two models (a and b) to generate a clean converted wave model (c).

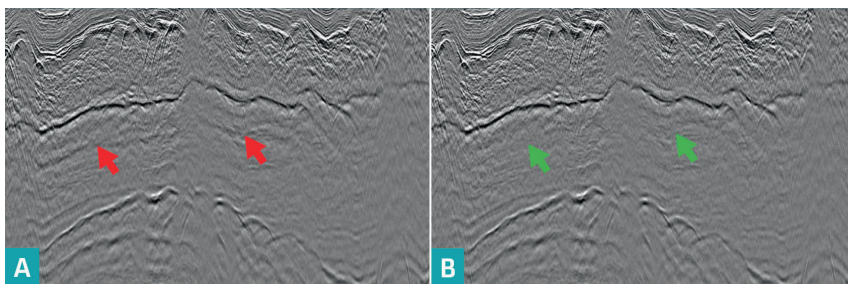


Figure 6 Stack output in the data domain without the converted wave attenuation flow applied (a) and with the converted wave attenuation flow applied (b).

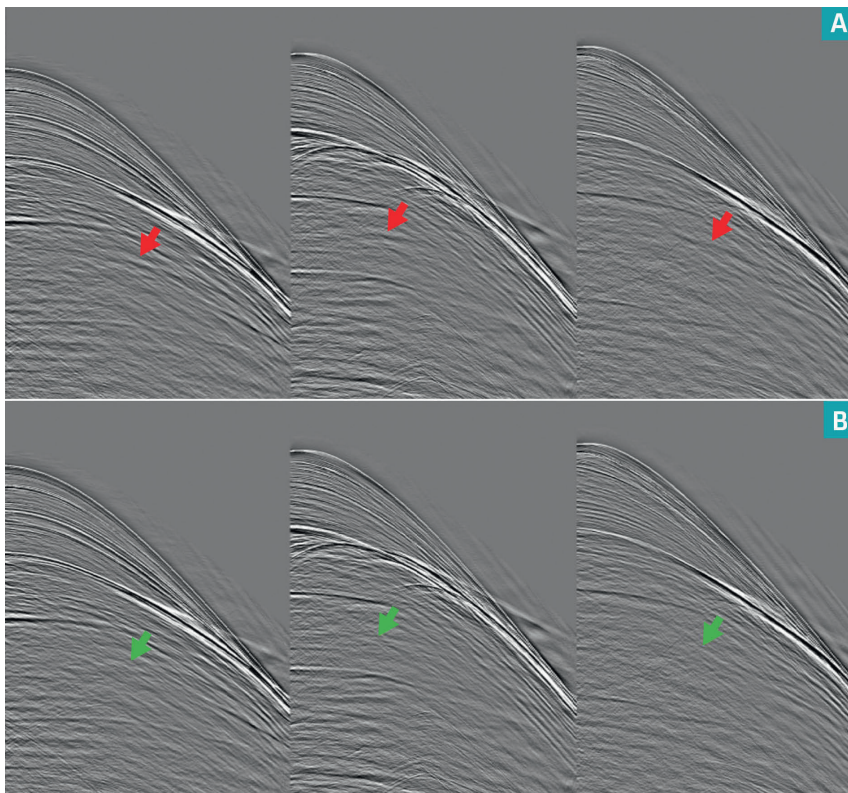


Figure 7 Raw shot gathers without the converted wave attenuation flow applied (a) and with the converted wave attenuation flow applied (b).

Assuming zero-offset raypaths, the ratio (r) can be expressed mathematically as follows (Lu et al., 2003):

$$r = \frac{\Delta t_{salt}}{\Delta t_{cw}} = \frac{\frac{2}{V_p}}{\left(\frac{1}{V_p} + \frac{1}{V_s}\right) - \frac{2}{V_p}} = 2 \left(\frac{V_s}{V_p - V_s}\right) \quad (1)$$

$$r = \frac{\Delta t_{salt}}{\Delta t_{cw}} = \frac{\frac{2}{V_p}}{\frac{2}{V_s} - \frac{2}{V_p}} = \left(\frac{V_s}{V_p - V_s}\right) \quad (2)$$

The ratio for asymmetrical mode can be calculated using eq (1) and its value is generally between 2 and 3, whereas the ratio for symmetrical mode can be calculated using eq (2). The value of the ratios in this case is significantly lower, between 1 and 1.5. This information aids the selection of the type of converted mode required during the forward modelling process.

The method proposed to suppress the converted mode is presented in Figure 4. The first step in the flow is to obtain a suitable interval velocity model for the P-wave data with an accurate salt layer geometry. Following this, a version of the velocity model containing the S-wave velocity within the salt body is built. The S-wave velocity is obtained by scanning for the velocity that flattens the converted mode energy at the same depth as the interpreted base salt. 3D Finite Difference shot modelling

is then performed using a single scattering approximation to produce modelled shot gathers corresponding to the wavefields (PSPP, PPSP and PSSP) resulting from conversion at the top salt and reflection from the base salt reflectors (Figure 5a). It can be clearly observed in Figure 5a that this model is not sufficient as diffractions from the top salt mask the converted mode energy, making it difficult to subtract from the input dataset. An additional 3D finite difference modelling step is performed to model P-waves without any reflection from the base salt reflectors (Figure 5b). A difference is produced of the model obtained from the two forward modelling processes, producing a clean converted mode only model (Figure 5c).

The difference represents the converted wave (C-wave) only model, and is adaptively subtracted from the input shot gather suppressing the recorded PSPP, PPSP and PSSP converted mode energy.

The adaptive subtraction is an important step in the workflow. This is required to compensate for small errors in modelled time and amplitude, which may be owing to either interpretation or errors in the velocity model used for forward modelling step. Intelligent adaptive subtraction (Perrier et al. 2017) was used to subtract the converted wave model from the input dataset. The

technique combines intelligently least square filtering in the time-space domain and a curvelet domain-based subtraction (Nguyen et al. 2017) to adapt the model more effectively. It preserves primary energy, which is absent in the model, by using a ‘true model’ adaptive subtraction technique.

The computed model from the first forward modelling step can be used to suppress the converted mode directly, but in this case the subtraction has to be done in the image domain where diffractions from the top-salt have collapsed and do not to mask the converted wave energy. Performing the additional modelling and difference phase allows a more effective suppression of the converted wave energy in the data domain.

Examples

Case study 1 – Egypt

The first case study comes from Egyptian waters in the eastern Mediterranean Sea. Seismic processing was performed on an area of approximately 4700 km², and comprised data from five separate acquisition surveys. The main contributing dataset to the seismic volume was acquired in 2017 by the PGS vessel M/V *Ramform Tethys*. The survey was acquired with a configuration using 14 dual-sensor streamers, each 9000-m long, towed at a depth of 25 m

and with a total surface spread width covering 1300 m. Two source arrays were used shooting at 25 m flip to flop. The nominal seismic acquisition bin size was 6.25 m by 25 m, with 80 fold of coverage.

The modelling of symmetrical modes (PSSP) was ignored in this case, owing to a lack of evidence of its presence in the recorded field data. The ratio (r), described in equations (1) and (2), was estimated at 2.2, inferring that the converted mode was recorded with only one of the up-coming or down-going wave-fields as an S-wave in the salt layer; either PSPP, or PPSP, or both (Figure 5). The velocity model for the modelling was generated using tomography in the post-salt section to estimate the sediment velocity. The salt layer velocity was estimated using a salt flooding methodology after interpreting the top salt reflection. The aim of this flooding step was to obtain optimal flatness of the base salt reflection. For this dataset, the P-wave velocity of the salt was estimated at 4200 m/s, whereas the S-wave velocity was estimated as 2400 m/s.

The result of the converted wave attenuation workflow is shown in both data and image domains. In Figure 6a, the red arrows clearly indicate the converted wave energy. As expected, the energy has the same phase response as the base salt reflection, but with a delayed recorded time. This is sometimes referred to as the base salt ghost reflection. Figure 6b shows the same

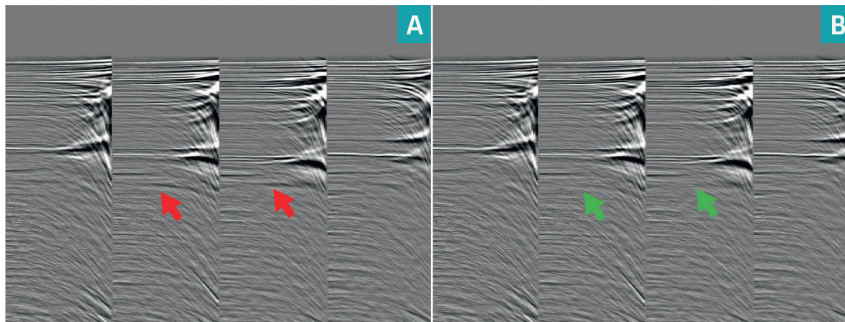


Figure 8 Depth migrated CDP gathers without the converted wave attenuation flow applied (a) and with the converted wave attenuation flow applied (b).

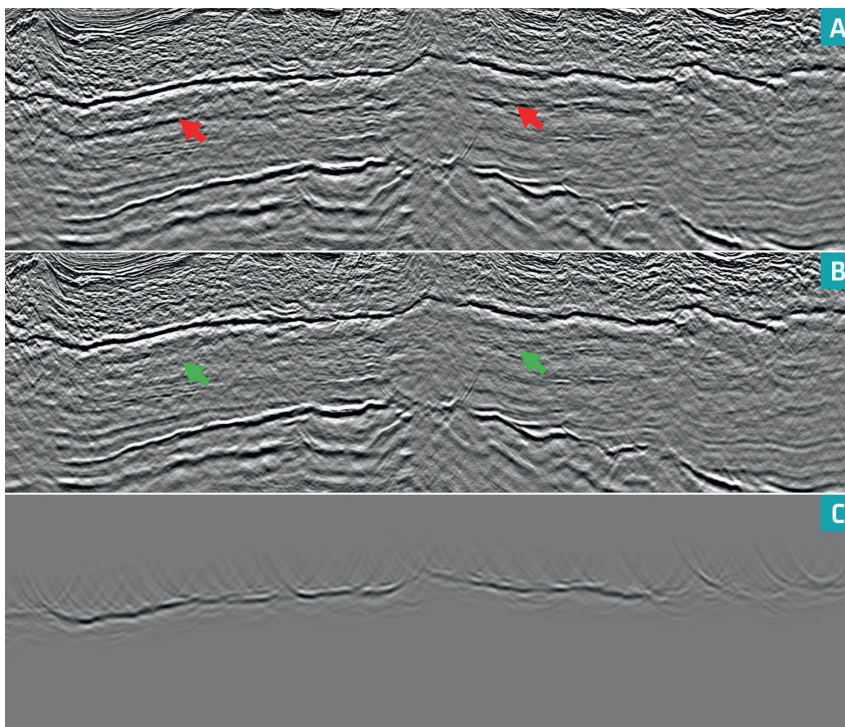


Figure 9 Depth migrated stacks without the converted wave attenuation flow applied (a); with the converted wave attenuation flow applied (b) and difference plot (c).

subsurface stack after the application of the converted wave attenuation workflow. The green arrows in Figure 6b point to the same location as the red arrows in Figure 6a. It is evident that the described workflow has successfully attenuated the converted wave energy. Figure 7 shows the result of the workflow in the data domain on common shot gathers. Converted waves are harder to identify in the shot records. However, it can be traced easily from the stack dataset. Arrows indicate where the recorded converted wave energy resides in the shot gathers. Again, it is clear that the converted wave energy has been attenuated by the proposed workflow.

Figures 8 and 9 show the results of the methodology in the image domain obtained by migrating data using a Kirchhoff algorithm. Figures 8a and 8b show the result on common depth point (CDP) gathers, where the converted wave has been marked with arrows. The move-out of this energy is quite small, approximately 100 ms at 8 km offset, making it difficult to filter using normal move-out based methods. Figures 9a and 9b show the same data after stacking. The effectiveness of the flow in attenuating recorded converted wave energy, which acts as noise in the

P-wave image, is self-evident. Figure 9c illustrates the difference of the application, showing the attenuated energy and its response to the migration operator.

Case study 2 – Cyprus

Data for the second case study were acquired for PGS MultiClient in Block 10 offshore Cyprus by PGS vessels *M/V Ramform Tethys* and *Hyperion*, commencing in 2016 and completing in 2017. The total area acquired was 6045 km². The data were acquired using a spread of 14 dual-sensor streamers each 9000-m long and separated by 100 m. Two sources were used with a 25 m flip to flop shooting interval.

The velocity model for the modelling was generated using tomography in the post-salt section to estimate the sediment velocity. During the velocity analysis for the salt bodies, it was observed that there were regions of dirty salt, requiring a slower average salt velocity than areas of clean salt. A spatially variable salt velocity was inserted with a background clean salt velocity of 4350 m/s, and slower velocities, in the regions containing dirty salt such that the gather flatness at the base salt, were optimized.

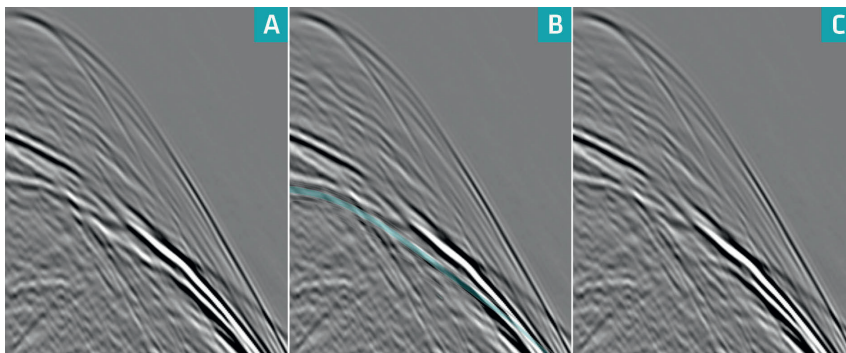


Figure 10 Raw shot gather showing the mode converted energy lying beneath the base salt reflector (a); raw shot gather with asymmetrical mode conversion model overlain (b) and shot gather after converted energy removed (c).

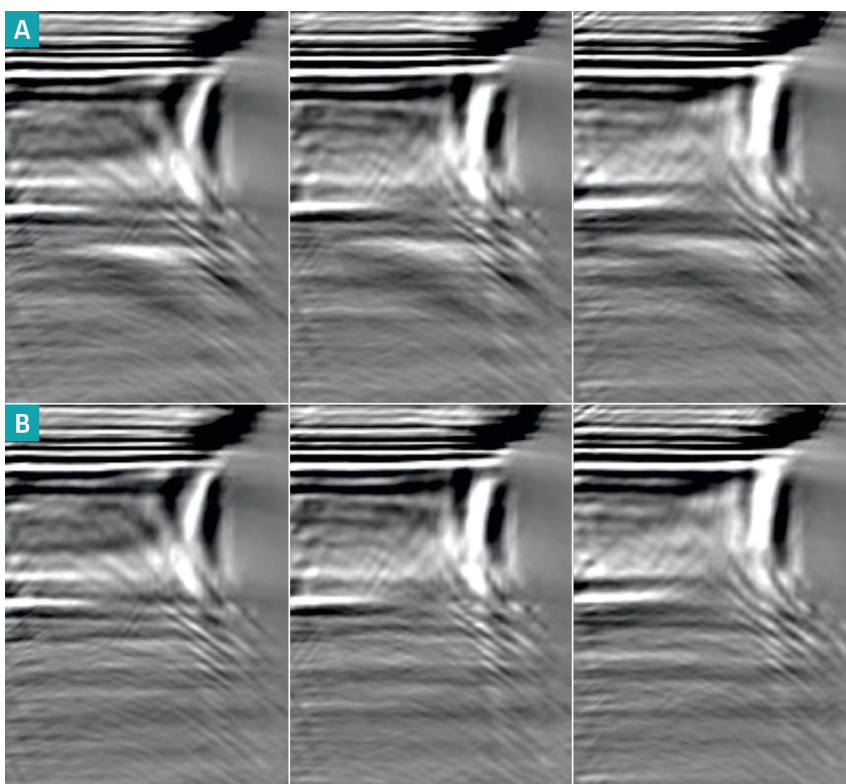


Figure 11 Depth migrated CDP gathers from before (a) and after (b) the mode conversion removal. The location of the mode converted energy is highlighted by the red arrows. Once the energy is removed the weaker amplitude primary events become more visible.

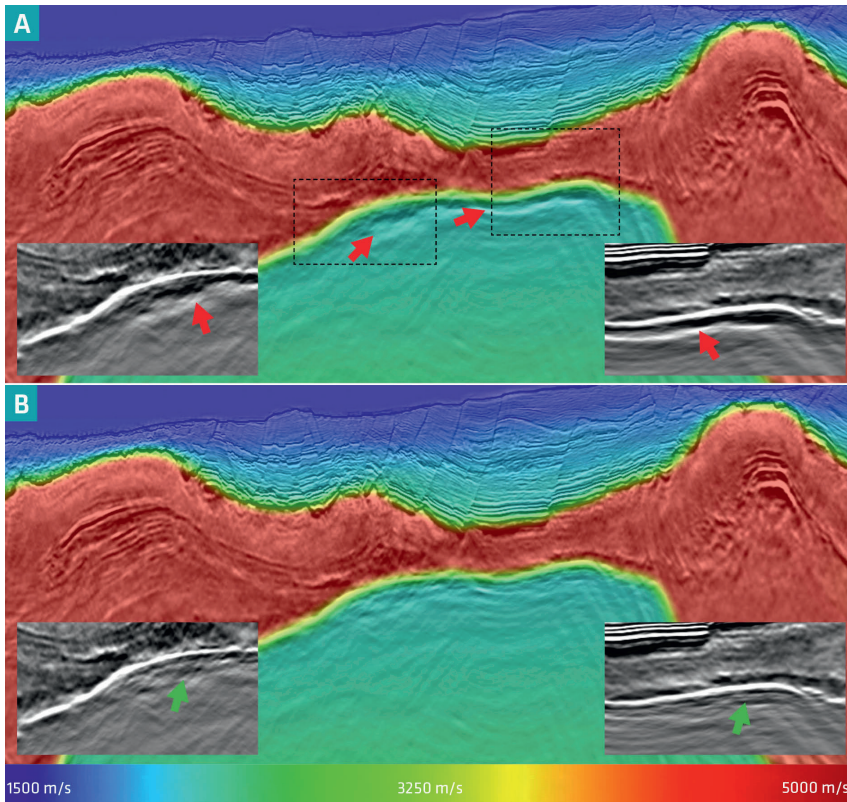


Figure 12 Depth migrated stacks from before (a) and after (b) the mode conversion removal. Migration velocities overlain. The location of the mode converted energy is highlight by the red arrows in a) and the primary that is now visible is highlighted by the greens arrows in b).

Using equations (1) and (2), the analysis of the depth of the converted energy below the salt versus salt thickness suggested that a V_p/V_s ratio of 1.8 was appropriate in this area; the S-wave salt velocity model used for the modelling was a scaled version of P-wave model in the salt.

Figure 10 shows a common shot gather from the survey area annotated with the location of the asymmetrical mode converted energy, and results after the mode converted energy has been removed. The effectiveness of the converted energy removal is clearly visible in the pre-stack data domain gathers. Figure 12 shows Kirchhoff depth stack images before and after the removal of the mode converted energy. As with the example from Egypt, the ‘ghost’ reflector under the salt is attenuated. This results in a cleaner pre-salt image, where primary P-wave energy dipping up against the base salt is revealed, and data interpretability is significantly improved, particularly as the base salt can form a trap to prospectivity in this area. The pre-stack data in Figure 11 also shows the elimination of the low-frequency converted wave energy. Attribute analysis on this data is contaminated by the noise from the mode transformation, where amplitudes analysis shows an inconsistent behaviour if the noise is not attenuated.

Conclusions

Converted wave energy following either asymmetrical (PSPP, PPSP) or symmetrical (PSSP) modes can significantly hinder data usage, particularly in salt provinces such as the eastern Mediterranean Sea, where prospectivity exists in the pre-salt section. We have demonstrated, in two distinct locations, a simple but effective approach that attenuates the offending noise, revealing the pre-salt reflectivity, and reducing risk associated with both data interpretability and attributes analysis.

Acknowledgements

The authors wish to thank PGS MultiClient for authorization to show examples from the different surveys acquired by PGS throughout the eastern Mediterranean. We would like to give special thanks to all the geophysicists from PGS who helped us in producing the results.

References

- Aal, A.A., El Barkooky, A., Gerrits, M., Meyer, H., Schwander, M. and Zaki, H. [2000]. Tectonic evolution of the Eastern Mediterranean Basin and its significance for hydrocarbon prospectivity in the ultradeepwater of the Nile Delta. *The Leading Edge*, **19**, 1086–1102.
- Ben-Avraham, Z., Ginzburg, A., Makris, J. and Eppelbaum, L. [2002]. Crustal Structure of the Levant Basin, Eastern Mediterranean. *Tectonophysics*, **346**, 23–43.
- Druckman, Y.B., Buchbinder, G. M., Martinotti, R., Tov, S. and Aharon, P. [1995]. The buried Afiq Canyon (eastern Mediterranean, Israel): a case study of a Tertiary submarine canyon exposed in Late Messinian times. *Marine Geology*, **123**, 167–185.
- Elbassiony, A., Kumar, J. and Martin, T. [2018]. Velocity model building in the major basins of the eastern Mediterranean Sea for imaging regional prospectivity. *The Leading Edge*, **37**(7), 519–528
- Gardosh, M. and Druckman, Y. [2006]. Seismic Stratigraphy, Structure and Tectonic Evolution of the Levantine Basin, Offshore Israel. *Geological Society, Special Publications*, **260**, 201–227.
- Garfunkel, Z. [1998]. Constraints on the origin and history of the eastern Mediterranean basin. *Tectonophysics*, **298**, 5–35.
- Gradmann, S., Hübscher, C., Ben-Avraham, Z., Gajewski, D. and Netzeband, G. [2005]. Salt tectonics off northern Israel. *Marine and Petroleum Geology*, **22**(5), 597–611.

- Huang, Y., Gou, W., Leblanc, O., Ji, S. and Huang, Y. [2013]. Salt-related converted-wave modeling and imaging study. *75th Annual EAGE Conference and Exhibition*, Tu 01 1
- Jones, I.F. and Davison, I. [2014]. Seismic imaging in and around salt bodies. *Interpretation*, **2**(4), SL1–SL20.
- Loncke, L., Gaullier, V., Mascle, J., Vendeville, B. and Camera, L. [2006]. The Nile Deep Sea Fan: An Example of Interacting Sedimentation, Salt Tectonics, and Inherited Subsalt Paleotopographic Features. *Marine and Petroleum Geology*, **23**, 297-315.
- Lu, R.S., Willen, D.E. and Watson, I.A. [2003]. Identifying, removing and imaging P-S-conversions at salt-sediment interfaces. *Geophysics*, **68**(3), 1052–1059.
- Netzeband, L., Gohl, G.K., Hubscher, P.C., Ben-Avraham, Z., Dehghani, A.G., Gajewski, D. and Liersch, P. [2006]. The Levantine Basin – Crustal Structure and Origin. *Tectonophysics*, **418**, 167-188.
- Nguyen, T. and Liu, Y.J. [2017]. Seismic noise attenuation using curvelet transform and dip map data structures. *79th Annual EAGE Conference and Exhibition*, We B3 08
- Ogilvie, J.S. and Purnell, G.W. [1996]. Effects of salt-related mode conversions on subsalt prospecting. *Geophysics*, **61**(2), 331–348.
- Perrier, S., Dyer, R., Liu, Y., Nguyen T. and Lecocq, P. [2017]. Intelligent adaptive subtraction for multiple attenuation. *79th Annual EAGE Conference and Exhibition*, We B3 03
- Roberts, G. and Peace, D. [2007]. Hydrocarbon Plays and Prospectivity of the Levantine Basin, Offshore Lebanon and Syria From Modern Seismic Data. *GeoArabia*, **12**(3).
- Robertson, A.H.F. [1998]. Tectonic significance of the Eratosthenes Seamount: a continental fragment in the process of collision with a subduction zone in the eastern Mediterranean (Ocean Drilling Program Leg 160). *Tectonophysics*, **298**, 63–82.
- Voogd, B. and Truffert, C. [1992]. Two-ship deep seismic soundings in the basins of the eastern Mediterranean Sea (Pasiphae cruise). *Geophysical Journal International*, **109**, 536–552.

ADVERTISEMENT





WWW.EAGE.ORG

Second EAGE/PESGB Workshop on Velocities

4-5 APRIL 2019 • LONDON, UNITED KINGDOM

Despite considerable improvements in seismic data quality and imaging algorithms, velocities and earth models remain the key challenge for depth prediction. Therefore, EAGE and PESGB have joined forces to establish a series of workshops to address this and other issues involved in velocities. In this second workshop, we will focus on all aspects of reducing uncertainties; including applications in seismic imaging, velocity model building, pore pressure prediction, depth conversion and drilling.

Submit your 1-2 pages abstract and present your ideas about this topic! Visit the event website via events.eage.org for a complete topics overview and other details.

Abstract Submission Deadline: **31 January 2019**

• Submit your Abstract!